Exploration and application of a liver-on-a-chip device in combination with modelling and simulation for quantitative drug metabolism studies†

Luca Docci, ‡§[ab] Nicolò Milani, iD §[ac] Thomas Ramp, iD [a] Andrea A. Romeo, iD [a] Patricio Godoy,[a] Daniela Ortiz Franyuti, iD [a] Stephan Krähenbühl,[b] Michael Gertz,[a] Aleksandra Galetin, iD [c] Neil Parrott[a] and Stephen Fowler iD *[a]

Microphysiological systems (MPS) are complex and more physiologically realistic cellular *in vitro* tools that aim to provide more relevant human *in vitro* data for quantitative prediction of clinical pharmacokinetics while also reducing the need for animal testing. The PhysioMimix liver-on-a-chip integrates medium flow with hepatocyte culture and has the potential to be adopted for *in vitro* studies investigating the hepatic disposition characteristics of drug candidates. The current study focusses on liver-on-a-chip system exploration for multiple drug metabolism applications. Characterization of cytochrome P450 (CYP), UDP-glucuronosyl transferase (UGT) and aldehyde oxidase (AO) activities was performed using 15 drugs and *in vitro* to *in vivo* extrapolation (IVIVE) was assessed for 12 of them. Next, the utility of the liver-on-a-chip for estimation of the fraction metabolized (f_m) *via* specific biotransformation pathways of quinidine and diclofenac was established. Finally, the metabolite identification opportunities were also explored using efavirenz as an example drug with complex primary and secondary metabolism involving a combination of CYP, UGT and sulfotransferase enzymes. A key aspect of these investigations was the application of mathematical modelling for improved parameter calculation. Such approaches will be required for quantitative assessment of metabolism and/or transporter processes in systems where medium flow and system compartments result in non-homogeneous drug concentrations. In particular, modelling was used to explore the effect of evaporation from the medium and it was found that the intrinsic clearance (CL_{int}) might be underestimated by up to 40% for low clearance compounds if evaporation is not accounted for. Modelling of liver-on-a-chip *in vitro* data also enhanced the approach to f_m estimation allowing objective assessment of metabolism models of different complexity. The resultant diclofenac $f_{m,UGT}$ of 0.64 was highly comparable with values reported previously in the literature. The current study demonstrates the integration of mathematical modelling with experimental liver-on-a-chip studies and illustrates how this approach supports generation of high quality of data from complex *in vitro* cellular systems.

1. Introduction

High quality estimates of pharmacokinetic (PK) parameters are essential during drug discovery for candidate selection and human dose predictions. Drug absorption, distribution, metabolism, and excretion (ADME) are the core PK processes which need to be optimized to obtain the desired clinical exposure. Multiple *in vitro* systems in conjunction with physiologically based pharmacokinetic (PBPK) modelling are routinely used for the experimental assessment and extrapolation of ADME properties. Primary hepatocytes cultured in either plated or suspension formats are often employed for the determination of the metabolic and transporter-mediated clearance, enzyme phenotyping and

[a] Pharmaceutical Sciences, Roche Pharma Research and Early Development, Roche Innovation Center Basel, Grenzacherstrasse 124, 4070, Basel, Switzerland. E-mail: stephen.fowler@roche.com; Tel: +41 61 688 5105

[b] Clinical Pharmacology & Toxicology, University Hospital, Schanzenstrasse 55, 4031, Basel, Switzerland

[c] Centre for Applied Pharmacokinetic Research, School of Health Sciences, Faculty of Biology, Medicine and Health, University of Manchester, UK

† Electronic supplementary information (ESI) available. See DOI: 10.1039/d1lc01161h

‡ Current Affiliation: Idorsia Pharmaceuticals Ltd, Hegenheimermattweg 91, 4123, Allschwil, Switzerland.

§ These authors contributed equally to this work.

metabolite identification. However, established *in vitro* assays still leave gaps in the quantitative translation which can potentially be addressed by the introduction of novel cell culture techniques. One limitation of hepatocytes cultured in a 2D format is the rapid loss of enzyme activity during the experiment which hinders accurate prediction of metabolic clearance, especially for metabolically stable drugs.[1,2] Additional limitations include the assessment of other ADME-related drug properties such as biliary and sinusoidal efflux,

accurate *in vitro* to *in vivo* scaling of active uptake clearance for substrates of drug transporters, prediction of *in vivo* relevant metabolites for metabolically stable drugs, and the reliable prediction of time-dependent inhibition and induction.[2–5] Microphysiological systems (MPS) hold promise to address more complex *in vitro* ADME, toxicology and pharmacology questions in a more physiologically relevant manner.[6,7] The PhysioMimix liver-on-a-chip is a microfluidic device that enables continuous perfusion of the hepatocytes
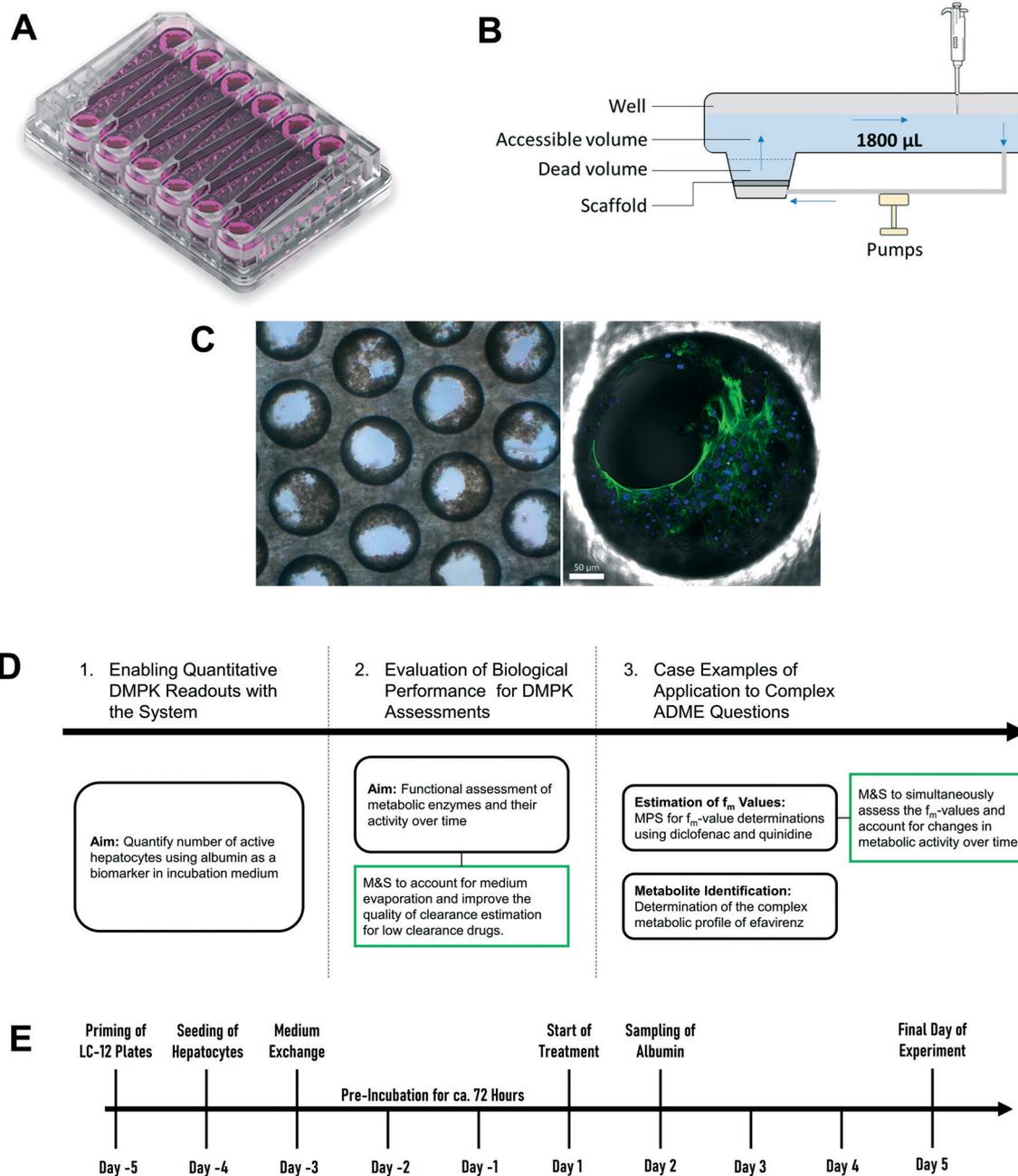
Fig. 1 Schematic representation of A) picture of the LC12 plate (©CN Bio Ltd., reproduced with permission); B) representation of the well in the LC12 plate which highlights the micropump system and the positon of sampling; C) scaffold and seeded hepatocytes: bright field light microscopy (left), and confocal microscopy (right) (BF, nuclei-DAPI and actin-phalloidin Alexa 488). D) The study outline and E) default procedure of plate preparation and experimental time course for the evaluation of CP, UGT and AO activity in the liver-on-a-chip. DMPK: Drug metabolism and pharmacokinetics; M&S: modelling and simulation; MPS: microphysiological system; f_m: fraction metabolized by individual enzyme isoforms.

to provide nutrients, oxygen, and mechanical stimuli through the shear stress of the media flow (Fig. 1).[8] The system used is closely related to the system previously described in a proof of principle study by Tsamandouras *et al.* who examined inter-individual variation in diclofenac metabolism *in vitro* and modelled this to the *in vivo* situation.[9] Vivares and colleagues[10] demonstrated prolonged maintenance of cell phenotype and higher metabolic activity in the liver-on-a-chip compared to 2D-cultured plated hepatocytes by using the same hepatocyte lot in both *in vitro* formats. Sarkar and colleagues[11] simultaneously assessed the metabolic profile as well as complex metabolite toxicity of diclofenac by combining primary human hepatocytes and Kupffer cells. Rubiano and colleagues[12] tested the ability of the liver-on-a-chip device to reproduce drug-induced hepatotoxic effects, metabolism, and intracellular accumulation and, importantly, demonstrated reproducibility of the experiments. The system is attractive for ADME applications as it offers the capability to seed a high number of hepatocytes per incubation chamber (referred to hereafter as "well"), has substantial medium volume enabling multiple drug concentration measurements and a growing body of prior evaluation data.[9,13,14] Despite these promising initial efforts, integration of MPS into pharmaceutical development workflows still requires verification that the platforms fulfil minimum requirements for ADME studies. The cells cultured in the liver-on-a-chip format need to demonstrate a physiologically relevant and stable phenotype[2,15] and, in addition, the results generated in MPS need to be robust and reproducible. Only after demonstration of these attributes and a broader validation including diverse molecules, can the systems be considered for more complex studies and for adoption by pharmaceutical companies.

The current study aimed to expand the evaluation of liver-on-a-chip system for applications in the drug metabolism and pharmacokinetic (DMPK) area, as illustrated in the framework in Fig. 1D. Firstly, the seeding efficiency of the system was determined by measuring the number of active hepatocytes residing in the scaffold. This evaluation is essential for quantitative translation of data from *in vitro* to *in vivo*, since the assumption that all cells seeded into a system are retained and active can be highly inaccurate. To allow this analysis to be performed in a non-invasive manner, albumin production rate was established as a surrogate marker for cell number estimation. Secondly, this study assessed the functional activity using multiple drug compounds known to be substrates of important drug metabolizing enzymes such as cytochromes P450 (CYPs), UDP-glucuronosyltransferases (UGTs), and aldehyde oxidase (AO). Thirdly, more complex endpoints were investigated, namely metabolite identification and fraction of drug metabolized *via* a single enzyme pathway (f_m), to demonstrate the potential of the liver-on-a-chip system. Modelling and simulation has been applied throughout as an essential part of experiment planning and data evaluation.

2. Experimental

2.1 Materials

Ketoprofen, zidovudine, dextromethorphan, dextrorphan, diclofenac, repaglinide, carbazeran, irinotecan, telmisartan, and quinidine were purchased from Sigma-Aldrich (St. Louis, MO, USA). Lorazepam, naloxone, 4′-hydroxydiclofenac, diclofenac-glucuronide, 3-hydroxyquinidine, 4-hydroxycarbazeran, naloxone-glucuronide, efavirenz, 7-hydroxyefavirenz, telmisartan-glucuronide, and posaconazole were purchased from Toronto Research Chemicals (Toronto, Canada). Cryopreserved hepatocyte recovery medium, William's E medium, primary hepatocyte plating supplements, primary hepatocyte maintenance supplements, and human hepatocytes (lot: Hu8264) were purchased from Thermo Fisher Scientific (Grand Island, NY, USA). Oxazepam, midazolam, and 1′-hydroxymidazolam were synthesized at F. Hoffmann-La Roche Ltd. (Basel, Switzerland). All CN Bio components (controller, docking station, and drivers) and consumables (LC-12 plates) were acquired from CN Bio Innovations (Cambridge, UK) (Fig. S1†).

2.2 Preparation of LC-12 plates and seeding of cryopreserved human hepatocytes

The diagram in Fig. 1E depicts the time scale of the process from plate preparation to the experiment. Detailed descriptions of the priming of the plates, the seeding process of the hepatocytes, and the media exchange program are provided in Supplementary Information. Briefly, five days before the start of the experiment (day − 5), LC-12 plates were primed by flooding the microchannels with plating medium (William's E medium containing 5% fetal bovine serum, 1 μM dexamethasone, 100 U mL^{-1} penicillin, 100 μg mL^{-1} streptomycin, 4 μg mL^{-1} human recombinant insulin, 2 mM GlutaMAX™, 15 mM HEPES). The day after (day − 4), hepatocytes were seeded on the scaffolds of the LC-12 plates. Primary cryopreserved human hepatocytes (one vial per LC-12 plate) were thawed and suspended in cryopreserved hepatocyte recovery medium. Supernatant was aspirated after centrifugation (100 G for 10 minutes) and hepatocytes were re-suspended in 3 mL plating medium. Cells were counted with a hemocytometer (Bioswisstec Ltd., Schaffhausen, Switzerland) and seeded at between 400 000 and 650 000 hepatocytes per well, depending upon the individual experiment (consensus: 600 000 cells per well). Plates were incubated at 37 °C in a 5% CO$_2$ atmosphere overnight to allow for the attachment of hepatocytes. The media was changed after attachment of the cells to the scaffold (at day − 3) to maintenance medium (William's E medium containing 0.1 μM dexamethasone, 50 U mL^{-1} penicillin, 50 μg mL^{-1} streptomycin, 6.25 μg mL^{-1} human recombinant insulin, 6.25 μg mL^{-1} human transferrin, 6.25 ng mL^{-1} selenous acid, 1.25 mg mL^{-1} bovine serum albumin, 5.35 μg mL^{-1} linoleic acid, 2 mM GlutaMAX™, 15 mM HEPES) and cells were pre-

incubated without media exchange for three days at 37 °C in a 5% CO_2 atmosphere until the first treatment day (day 1).

2.3 Quantification of cell number

On day – 4 of each experiment the remaining hepatocyte suspension not needed for seeding was used to investigate the total protein content per million hepatocytes. The hepatocyte suspension was diluted with 20 mL PBS and centrifuged at 100G for 10 minutes. The supernatant was aspirated and the hepatocyte pellet was lysed with 5 mL PBS containing 1% Triton-X for twenty minutes. Total protein content was measured using the Pierce™ BCA Protein Assay Kit (Thermo Fisher Scientific).

To relate the total cellular protein to the albumin production on day 2, three control wells in each experiment were used to determine the number of hepatocytes *via* lysis of the cells, assuming that all attached cells remained viable. By using the measured albumin concentration in the medium of the respective wells on day 2 (24 hours after media exchange at day 1) the normalized albumin production rate was calculated according to eqn (1):

$$\text{Albumin production rate } (\mu g_{ALB} \text{ per day per } 10^6 \text{ cells}) = \frac{C_{alb} \cdot V_{med}}{N_H \cdot t} \tag{1}$$

where C_{alb} is the concentration of albumin (in $\mu g \ \mu L^{-1}$) in the medium after 24 hours (t), V_{med} is the volume of medium (1800 μL) and N_H is the number of hepatocytes (expressed in

million cells) determined in the lysates from the control wells by protein concentration. The average albumin production rate calculated from the control wells was then used to derive the number of hepatocytes in the remaining wells based on the measured albumin concentrations in the medium. This was performed separately for each experiment, compensating for any changes in albumin generation rate between experiments performed on different occasions or for different culture durations.

The albumin concentration was measured using the human albumin ELISA kit (Immunology Consultants Laboratory, Inc., Portland, USA) and total protein was measured using the Pierce™ BCA protein assay kit to assess the number of cells in the control wells (Thermo Fisher Scientific, Grand Island, NY, USA). A detailed protocol about the lysis of the hepatocytes in the scaffolds of the control wells is provided in the Supplementary Information.

2.4 Assessment of drug metabolism capability

The major enzymes involved in the metabolism of the selected drug molecules are summarized in Table 1. Drug concentrations, time points of medium sampling, and sampling volumes are summarized in ESI† Table S1. On the first study day (day 1), the maintenance medium was replaced with a fresh maintenance medium containing the test drugs with a total volume of 1800 μL (200 μL dead volume plus 1600 μL added volume). Afterwards, no additional media exchanges were performed during the time

Table 1 Comparison of unbound hepatic intrinsic clearance values calculated from *in vivo* studies with extrapolated unbound *in vivo* intrinsic clearance from liver-on-a-chip data for 12 compounds. The R_{BP}, fu$_{plasma}$ and observed *in vivo* CL$_{int}$ were taken from the references provided. The mean *in vitro* unbound CL$_{int}$ and standard deviation are obtained using the fu$_{inc}$ which was either measured or calculated as indicated. *In vitro* data for carbazeran and irinotecan which were not included in the IVIVE were also reported in the table

Compound	Major metabolic enzymes	fu$_{plasma}$	R_{BP}	fu$_{inc}$	*In vitro* CL$_{int,u}$ μL per min per million cells	*In vivo* CL$_{int,u}$ Predicted mL/min/kg	*In vivo* CL$_{int,u}$ Observed	Fold error[g]
Carbazeran	AO (ref. 52)			0.74[b]	12 ± 1[e]			
Dextromethorphan	CYP2D6/3A4 (ref. 53)	0.72	1.5	0.77[b]	20 ± 2[e]	51	576 (ref. 25)[f]	0.089
Diclofenac	CYP2C9, UGT2B7 (ref. 17, 54)	0.010	0.55	0.045[a]	95 ± 9[d]	4	561 (ref. 25)	0.43
Irinotecan	CES[36]			0.76[a]	0.92 ± 0.04[c]	2.4		
Lorazepam	UGT2B7/15 (ref. 55)	0.11	1.0	0.80[b]	2.1 ± 0.3[e]	6.5	14 (ref. 25)	0.46
Midazolam	CYP3A4/5 (ref. 56)	0.031	0.55	0.10[a]	219 ± 23[e]	579	440 (ref. 21)	1.3
Naloxone	UGT2B7 (ref. 37)	0.56	1.22	0.87[a]	65 ± 2[e]	167	200 (ref. 21)	0.84
Oxazepam	UGT1A9/2B15 (ref. 57)	0.045	1.1	0.60[b]	14 ± 1[e]	37	34 (ref. 25)	1.1
Posaconazole	UGT1A4 (ref. 58)	0.017	1.0	0.37[b]	8.0 ± 2.0[e]	25	148 (ref. 20)	0.17
Quinidine	CYP3A4/5 (ref. 59)	0.13	0.87	0.63[a]	12 ± 2[d]	31	61 (ref. 25)	0.50
Repaglinide	CYP2C8/3A4 (ref. 39, 60)	0.014	0.60	0.36[b]	5.5 ± 1.7[e]	14	1380 (ref. 21)	0.010
Telmisartan	UGT1A3 (ref. 61)	0.005	1.0	0.15[a]	64 ± 8[e]	197	4519 (ref. 20)	0.044
Tolbutamide	CYP2C9 (ref. 35)	0.024	0.75	0.48[a]	1.2 ± 0.1[c]	3.1	3.6 (ref. 25)	0.88
Zidovudine	UGT2B7 (ref. 62)	0.74	0.99	0.98[b]	1.7 ± 0.5[e]	5.2	66 (ref. 20)	0.079

[a] Measured data. [b] Calculated data from fu$_{plasma}$, K_a in human serum albumin or bovine serum albumin (ESI† Table S5). [c] *In vitro* CL$_{int,u}$ were estimated by evaporation model of triplicate measurements with the respective ± SD. [d] *In vitro* CL$_{int,u}$ were estimated by modelling of triplicate measurements with the respective ± SD. For quinidine and diclofenac CL$_{int}$ from model 4 and 6 were respectively used. [e] *In vitro* CL$_{int,u}$ were estimated by mono-exponential decay of the substrate in triplicate measurements with the respective ± SD (eqn (3)). [f] The observed CL$_{int,u}$ was evaluated from oral administration assuming the intestinal availability and fraction absorbed equal to 1.[25] The unbound plasma and bold plasma ratio were taken from Lutz *et al.*[63] and Silva *et al.*,[64] respectively. [g] Fold error was calculated as a ratio between predicted and observed CL$_{int}$.

course of the experiment. The media was first allowed to distribute into the whole well for at least half an hour before the first sample was taken. At different time points, media samples were removed and quenched in acetonitrile containing internal standard (128 ng mL^{-1} D$_6$-midazolam for all test compounds), centrifuged at 6200 G for 10 minutes at 4 °C and stored at −20 °C until preparation for measurement in liquid chromatography tandem mass spectrometry (LC-MS/MS). Drug concentration was measured in triplicate for each compound. To determine the depletion of the probe substrates, the natural logarithm of the drug concentration in the incubation samples was plotted against time and linear regression analysis was applied using GraphPad Prism version 7.04 for Windows (GraphPad Software, La Jolla, CA). The *in vitro* intrinsic clearance (CL$_{int}$) was calculated from the depletion rate constant (k) of the linear regression (min^{-1}) for each well individually and assuming a rapid passive diffusion into the cells:

$$CL_{int} \ (\mu L \ per \ min \ per \ million \ cells) = \frac{k \times V_{med}}{N_H} \quad (2)$$

where V_{med} was 1800 μL, and N_H is the number of cells estimated from the measured albumin production rate in the respective wells.

In order to determine the tolerance of the system to repeated wash-out and re-use, measurement of compound depletion was performed repeatedly over four days (*i.e.* day 1, day 2, day 3, and day 4) with a washing step after every 24 hours before each incubation. This investigation of the repeated use activity retention was conducted for midazolam, diclofenac, repaglinide, carbazeran, quinidine, dextromethorphan, and naloxone. The retention of metabolic activity was assessed by comparing the depletion rates for the drug molecules at the different days (Fig. S2†).

2.5 Determination of *in vitro* intrinsic clearance for drugs with high metabolic stability

Three compounds with a high metabolic stability (tolbutamide, irinotecan, and ketoprofen) were selected to assess the impact of prolonged incubation times on the determination of the *in vitro* intrinsic clearance. Concentrations, sampling time points, and sampling volumes are summarized in ESI† Table S1. Incubations were run for 96 hours without performing media exchange during the time course of the experiment.

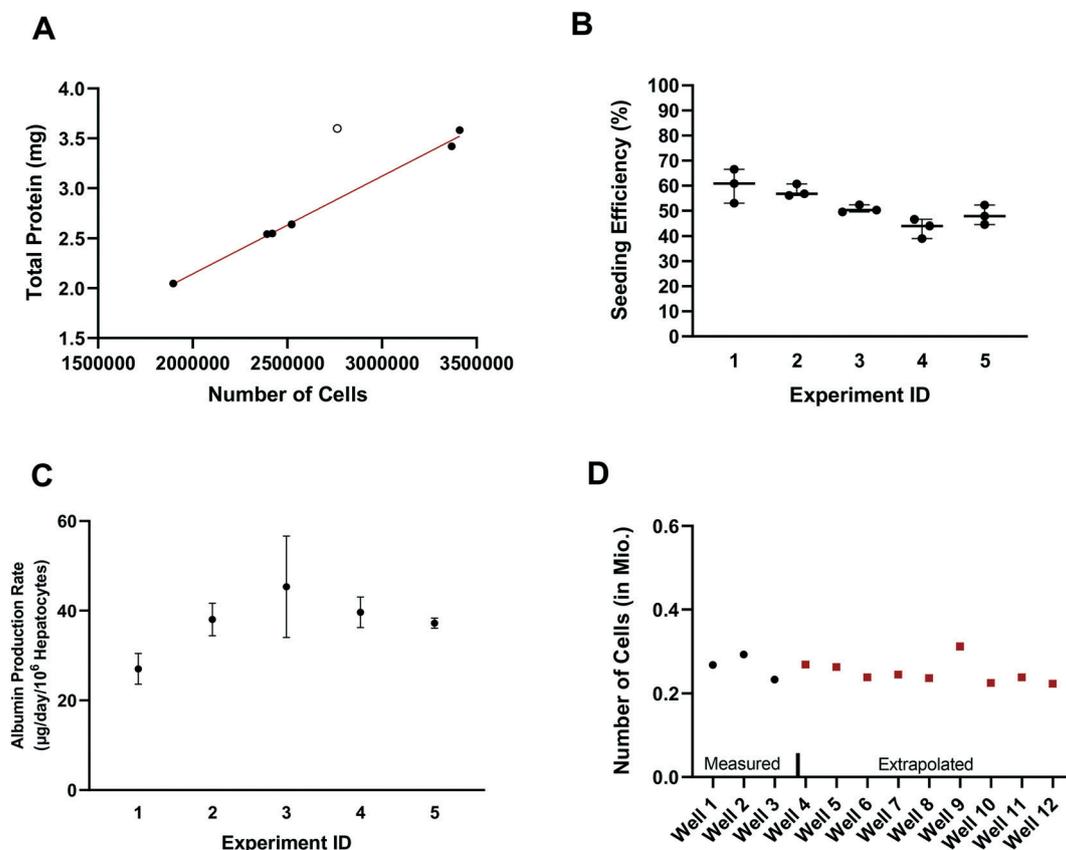For such prolonged incubations, evaporation from the medium may have an impact on the calculated intrinsic

Fig. 2 A) Correlation between total protein and number of cells. Data shown as filled circles were used for the correlation. B) Seeding efficiency of the experiments comparing the initial amount of hepatocytes seeded and the measured total protein amount at day 1 of the experiment in control wells. Number on the *x*-axis indicates the experiment number. C) Albumin production rate measured in three dedicated control wells in five different experiments as mean ± SD. D) Measured (black dots) and interpolated (red squares) number of cells in different wells in an example experiment.

A

B

C

D
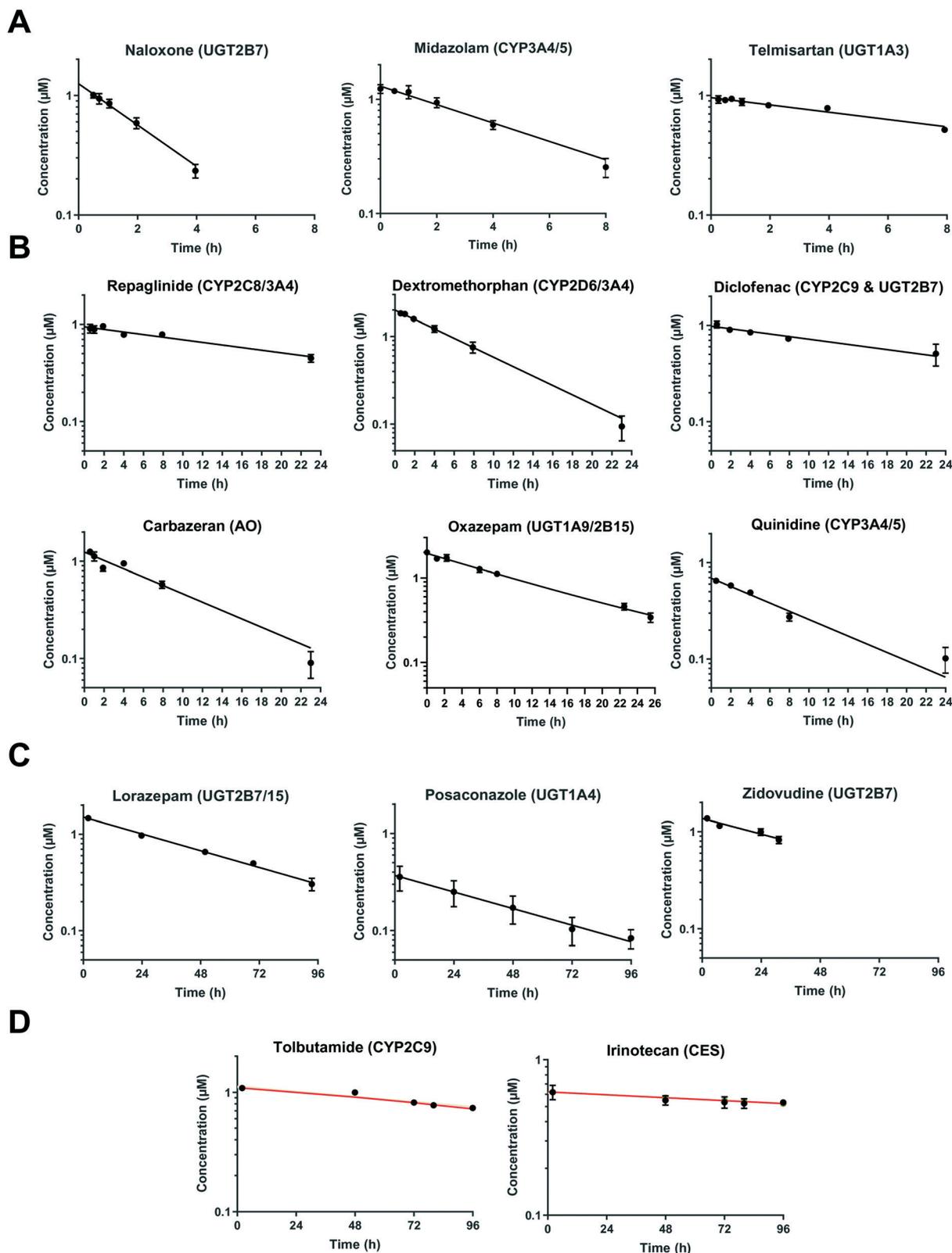
Fig. 3 Drug concentration in media plotted *versus* incubation time. A) Midazolam, naloxone, and telmisartan were incubated up to 8 h. The sample of naloxone after 4 h were not reported since it was below the limit of quantification. B) Diclofenac, quinidine, repaglinide, dextromethorphan, oxazepam, and carbazeran were incubated for up to 24 h. C) Lorazepam, zidovudine, and posaconazole were investigated for more than 24 h and linear regression was applied for the CL_{int} estimation. D) Low turnover compounds (tolbutamide and irinotecan) were incubated for 96 h and the evaporation model was used to estimate CL_{int} (model fit reported with red line). All data are shown on a log scale as a mean of triplicates with the respective standard deviation. Incubation at day 1 was reported for the compounds tested successively over 4 days (diclofenac, midazolam, quinidine, dextromethorphan, and carbazeran). The specific sampling points for each compound are reported in the ESI.†
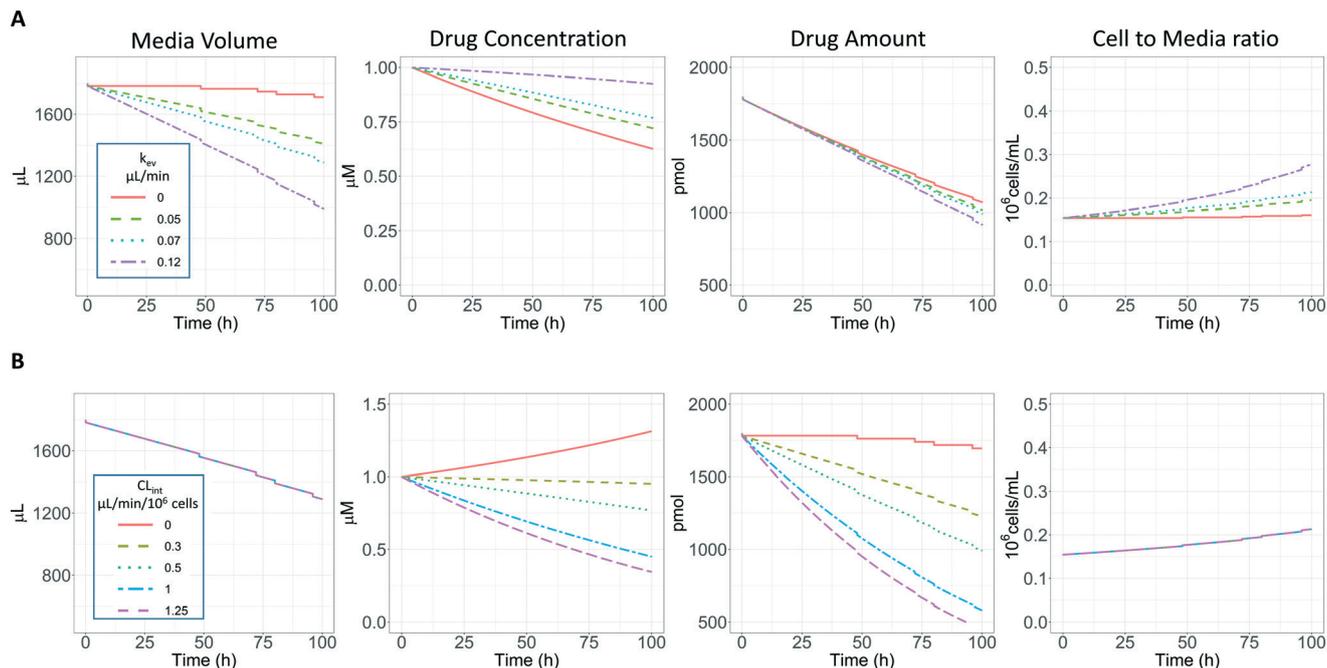
Fig. 4 A) Representation of the effect of evaporation and sampling on the media volume, drug substrate concentration, drug amount and cell to media ratio over 96 h of incubation with PhysioMimix liver-on-a-chip. Four different k_{ev} were evaluated (0, 0.05, 0.07, and 0.1 µL min^{-1}) with a CL_{int} of 0.5 µL per min per million cells and a sampling volume of 18 µL. B) Representation of the effect of CL_{int} (0, 0.3, 0.5, 1.0 and 1.25 µL min^{-1} 10^{-6}) on the same variables reported in panel a with a constant k_{ev} of 0.07 µL min^{-1}.

clearance, especially for metabolically stable drugs (Fig. 4A). The metabolism-driven reduction in drug amount may be partially masked by media evaporation which concentrates the remaining drug substance. In contrast, the amount of compound transformed may be greater in conditions of higher evaporation of the medium due to the increased drug concentration and more frequent passage through the cells (which may be considered as an increase in the number of cells per unit incubation medium volume, Fig. 4A). Fig. 4B illustrates the relationship between the CL_{int} the volume of medium, amount, concentration of the substrate, and cells/ volume ratio when k_{ev} is maintained (0.07 µL min^{-1}). In addition, Fig. 4 shows the impact of the sampling volume on the total media volume, amount, and cells/volume ratio as a sudden reduction of volume compared to the constant process of evaporation. The sampling volume does not immediately impact the concentration *vs.* time profile but has an effect over time and affects the number of data points which may be collected. In order to reduce the impact of the sampling volume in the actual experiments, it has been minimised to 18 µL considering the sample preparation and analysis processes. Therefore, a more complex model (referred to here as the evaporation model) is proposed to account for medium evaporation and sampling while estimating the CL_{int}. For comparison, the linear model (eqn (3) without evaporation) and the evaporation model (eqn (3) and (4)) were both used to fit the observed concentration-time profiles and to estimate the *in vitro* intrinsic clearances.

The evaporation model assumed that the combination of media circulation and passive diffusion into cells is rapid

and a one-compartment model was sufficient to describe the concentration of drug in the medium (full model is detailed in ESI,† *In silico* modelling section). Concentrations of the drug at different time points were measured and the amount of drug in the system calculated by multiplying the drug concentration by the system media volume. For modelling, the change in amount of drug in the system with time is described by eqn (3):

$$\frac{dA}{dt} = -CL_{int} \cdot fu_{inc} \cdot N_H \cdot C(t) \tag{3}$$

where fu_{inc} is the unbound fraction of drug in the incubation medium; C and A are the concentration and amount of drug, respectively, at given time points t. Media volume decreased over time due to evaporation and sampling as described by eqn (4):

$$V(t) = V_i - k_{ev} \cdot t - ns(t) \cdot V_s \tag{4}$$

where V_i represents the initial volume (1818 µL) and t represents the time. The evaporation constant k_{ev} (in µL min^{-1}) was experimentally determined by measurement of the volume of the incubation medium in all wells at the final day of the experiment for the calculation of medium volume from medium weight. In addition, the sudden removal of medium and drug amount due to the sampling (18 µL per time point) was considered with the V_s term at the specific time-dependent sampling points ns (Fig. 4).

The k_{ev} was then calculated using eqn (5) by assuming a volume decrease following zero-order kinetics:

$$k_{ev} = \frac{V_i - V_f}{t_f} \tag{5}$$

where V_i, V_f, and t_f, represent the initial, final volumes per well, and the incubation time, respectively. The loss of medium due to sampling (V_s) and the dead volume (200 μL) remaining in the well after aspirating the medium were taken into account when deriving V_f.

2.6 Evaporation model exploration

In addition to their application for CL_{int} estimation from the observed *in vitro* data, the linear model and the evaporation model were also used to perform a preliminary *in silico* simulation assessment to test the adequacy of the two analyses. For this assessment, the evaporation model was applied to generate *in vitro* concentration-time profiles for a range of theoretical *in vitro* CL_{int} values from 0.3 to 1.25 μL per min per million cells and different rates of evaporation from 0.01 to 0.12 μL min^{-1}. The model used for all simulations included a constant number of hepatocytes (N_H = 275 000 cells per well) and random effects (ω) for N_H (CV = 20%) and k_{ev} (CV = 20%) which were based on our experience of experimental variability. In addition, the sampling volume of 18 μL was considered in the simulation in order to take into account the amount of substrate removed from the medium at the time of sampling. Moreover, a residual unexplained variability in the observed data was modelled with an exponential error of 10% represented by eqn (6).

$$C^i_{Obs} = C^i_{pred} \times e^{\varepsilon_i} \tag{6}$$

where C^i_{Obs} represents the observed concentration affected by ε_i which is the deviation from the population value for each time point.

In order to assess variability, 1000 concentration-time profiles were simulated with the evaporation model using the conditions described above and three replicates were randomly sampled from the full set of simulated data at time points up to 96 hours. The random sampling was repeated 100 times. CL_{int} values were then estimated by fitting either with the linear model (eqn (3) only) assuming $V(t)$ is constant and equal to V_i or with the evaporation model (details about the fitting procedure are available in Software and libraries for modelling section). The sampling times used for the fitting of both models were: 0, 48, 56, 80, and 96 h.

Finally, the accuracy of the estimated mean CL_{int} values was computed with the root-mean-square error (RMSE, eqn (7)) while the absolute average fold error (AAFE, eqn (8)) was used to evaluate the bias. In addition, the median of the uncertainty of 100 experiments were also evaluated. The percentage relative standard error (RSE) was evaluated and % RSE above 30% was considered as threshold of CL_{int} uncertainty; details are summarized in the ESI† (Fig. S4).

$$RMSE = \frac{\sqrt{\sum_{i=1}^{N}(x_i - \hat{x}_i)^2}}{N} \tag{7}$$

$$AAFE = 10^{\frac{1}{N}\sum_i \left| \log \frac{x_i}{\hat{x}_i} \right|} \tag{8}$$

where N is the number of observations, and x_i and $\hat{x}_i$ are the predicted and observed parameters respectively. In addition for this set of 100 random triplicates, the median of the distribution of the 100 estimated CL_{int} values was also evaluated. Finally, we evaluated in which experimental conditions of k_{ev} and CL_{int} the approximated linear model may be used to estimate CL_{int} with low bias.

2.7 Determination of fractions metabolized and metabolite formation for quinidine and diclofenac

Quinidine and diclofenac were incubated as described above and samples were taken at specific time points to measure drug disappearance and metabolite formation. The data for drugs and metabolites were subsequently analysed with different *in silico* models to estimate the fractions metabolised and rates of metabolite formation. The structure of the models is displayed in Fig. 7.

Four different *in silico* models with different levels of mechanistic detail were used to describe the observed concentration-time profiles of quinidine and 3-hydroxyquinidine. Model 1 assumed a single metabolic pathway and that quinidine depletion was solely due to 3-hydroxyquinidine formation. Model 2 considered also subsequent 3-hydroxyquinidine metabolism. Model 3 assumed that depletion of quinidine is due to the formation of 3-hydroxyquinidine and one or more additional primary metabolites[16] (*e.g.* quinidine N-oxide). The latter was also assumed by model 4 which was a combination of model 2 and 3.

For diclofenac, *in silico* modelling was applied to estimate simultaneously CL_{int} and contributions from oxidation (by CYP enzymes such as CYP2C9, CYP2C8 and CYP3A4) and glucuronidation (*e.g.* by UGT2B7) to overall metabolism ($f_{m,CYP}$ and $f_{m,UGT}$).[11,17] Two models were applied to describe the concentration-time profiles for diclofenac and its metabolites at different levels of mechanistic details (Fig. 7). Model 4 assumed the formation of 4′-hydroxydiclofenac and diclofenac-glucuronide, whereas model 5 considered also an additional but not measured primary metabolism pathway (*e.g.* 5′-hydroxydiclofenac formation). In order to define the best model for describing the experimental data, the Bayesian information criterion (BIC) was used for diclofenac and quinidine and their respective models 1–6. The model with the lowest BIC rank and strongest support from current literature information was selected for parameter estimation.
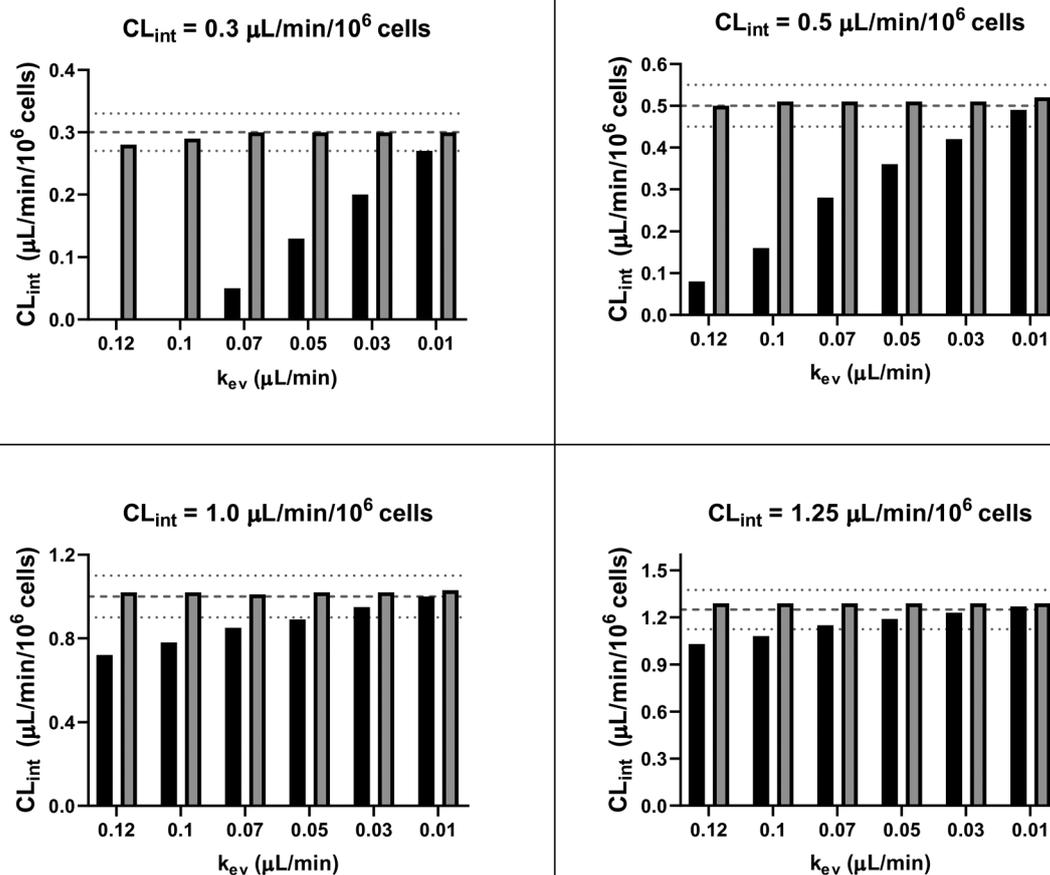
Fig. 5 *In silico* comparison of the estimated CL_{int} using the linear (black bars) and the evaporation (grey bars) models. The dashed lines represent the expected value for CL_{int} and the dotted lines its variance of ±10%. For CL_{int} value of 0.3 μL per min per million cells with k_{ev} of 0.12 and 0.10 μL min^{-1} the median of the estimated clearance with the linear model was negative and so the respective bars are not reported.

2.8 Protein binding

Fraction unbound in the incubations (fu_{inc} values) was determined in the maintenance medium using equilibrium dialysis against 133 mM phosphate buffer at pH 7.4, over 5 hours at 37 °C in a 5% CO_2 atmosphere, using a Teflon equilibrium dialysis plate (96-well, 150 μL, half-cell capacity) and cellulose membranes (12–14 kDa molecular weight cut-off) from HT-dialysis (Gales Ferry, Connecticut). Aliquots from the donor and receiver compartments were combined with buffer or blank media to make 10% media (v/v) matrix-matched samples, which were further prepared by the addition of acetonitrile-containing internal standard.

2.9 Sample preparation and liquid chromatography-mass spectrometry analysis

The drug concentration was measured with LC-MS/MS using the HTS CTC PAL autosampler together with Shimadzu pumps for the UHPLC system (Nexera X2) and a QTRAP5500 (AB Sciex) equipped with a TurboIonSpray source for the

mass spectrometry. Detections were made in positive or negative ion MRM mode and data processing was conducted with Analyst software (version 1.6.2, SCIEX). ESI† Tables S2 and S3 provides more detailed information about the parameter settings in the MRM mode, analytical columns, mobile phases, sampling volumes, flow rates, and retention times.

For the protein binding assessment the samples were quantified by liquid chromatography coupled with triple quad mass spectrometry. After correcting for dilution during sample work-up, peak area ratios of analyte *vs.* internal standard were used in the calculation of unbound fraction. All recovery values were in the range 80–120%. No observable volume shift was seen over the duration of incubation and potential volume shifts were therefore not factored into the free fraction calculations.

2.10 Metabolite identification for efavirenz metabolism

Metabolite identification was performed using the same experimental conditions reported for low clearance

compounds. The incubation time was 96 h with sampling times were 0, 48, 72, 80, 96 h and number of cells around 300 000 for the three replicates. Each sample was diluted and the 10 μL of supernatant was used for LC-MS/MS analysis. For the instrumental analysis were used: Dionex Ultimate 3000 RS System UHPLC (ThermoFisher), with injection system a PAL HTC xt Autosampler (CTC), and the column Waters Acquity UPLC BEH C18 (1.7 μm, 2.1 × 100 mm). The column temperature was maintained at 40 °C. As chromatography solvent A: 0.1% formic acid in water and solvent B: 0.1% formic acid in acetonitrile with a gradient and flow rate of 0.4 mL min⁻¹. The mass analyser was a ThermoFisher Q Exactive hybrid quadropole-orbitrap mass spectrometer equipped with Xcalibur version 4.2 and the Tune 2.9 software package. The scan event cycle consisted of acquisition of one full mass spectrum (m/z 135 to 1200) at a resolving power of 70 000 (@m/z 200), followed by data-dependent MS/MS scans. The ESI conditions were: spray voltage: 3500 V, probe heater temperature 300 °C, capillary temperature 320 °C, sheath gas 35, and auxiliary gas 10. The measure of the drug compound and its metabolites were based on the peak area intensity. The % peak area of metabolites was estimated by comparison of peak areas of MS ion intensities. This semi-quantitative approach is based on several simplified assumptions (equimolar response of different analytes, no matrix effect, *etc.*) and consequently, it cannot be excluded that in some cases the semi-quantitative data will be different to data generated by validated bioanalytical methods using individual reference compounds or by structure independent radioactivity measurements. 7-Hydroxyefavirenz (M6) was used as standard to separate it from the regioisomer metabolite 8-hydroxyefavirenz (M1).

2.11 Prediction of *in vivo* intrinsic clearance

In vitro to *in vivo* extrapolation (IVIVE) of the metabolic clearance was performed for all compounds that were investigated in this study except irinotecan, ketoprofen and carbazeran. Ketoprofen was excluded due to poor *in vitro* PK profile. Irinotecan was excluded due to the complex pharmacokinetics involving the lactone and inactive carboxylate forms, which are dependent on the pH and albumin concentration.[18] Carbazeran was excluded because of high extrahepatic extraction.[19] For compounds that were measured in the repeated incubation experiment, only the CL_{int} derived on the first day was used.

The measured *in vitro* CL_{int} values were transformed to the predicted unbound *in vivo* CL_{int} using eqn (9):

$$\text{Pred.}in\ vivo\ CL_{int,u}\ (\text{mL min}^{-1}\ \text{kg}^{-1}) = \frac{In\ vitro\ CL_{int} \cdot HC \cdot LW}{fu_{inc}} \quad (9)$$

where the hepatocellularity (HC) was 120 million hepatocytes per gram of liver,[20] LW was the average weight of the liver per kg of body weight which was taken as 21.4 g liver per kg,[21] and fu_{inc} was the unbound fraction of drugs investigated in the medium.

When no measured unbound fractions in the incubation medium (fu_{inc}) were available (zidovudine, lorazepam, posaconazole, dextromethorphan, repaglinide, and oxazepam), the values were estimated from reported plasma protein binding values, albumin unbound fraction or association constant with BSA (ESI† Table S5). When plasma or human albumin data were used, the compound was assumed to have the same affinity between human albumin and BSA. The $fu_{inc,pred}$ estimated by the plasma unbound fraction eqn (10) was used:

$$fu_{inc,pred} = \frac{1}{1 + \dfrac{1 - fu_p}{C_{alb} \cdot fu_p} C_{BSA}} \quad (10)$$

where fu_p is the reported unbound fraction of the drug in the plasma and C_{alb} the concentration of human albumin in plasma (42.5 g L⁻¹) and C_{BSA} is the concentration of BSA in the medium.

The compounds were assigned to the ECCS (extended clearance classification system) using the available literature. Midazolam, dextropmetorphan, repagnalide, quinidine, posaconazole, tolbutamide, and diclofenac classification were collected from Umehara *et al.*[22] Naloxone, zidovudine, lorazepam, and oxazepam from Docci *et al.*[23] and telmisartan from Tess *et al.*[24]

2.12 Calculation of observed *in vivo* intrinsic clearance

In vivo hepatic clearance values were collected from previously published literature reports. Whenever possible, clearance estimates derived after an intravenous administration were used. One exception was dextromethorphan, where oral clearance was used and the intestinal availability and fraction absorbed were set equal to 1.[25] Metabolic plasma clearance was calculated from total plasma clearance using eqn (11):

$$CL_{H,p}\ (\text{mL min}^{-1}\ \text{kg}^{-1}) = CL_p \cdot f_{met} \quad (11)$$

where CL_p is the total metabolic plasma clearance and f_{met} is the fraction metabolized by hepatic metabolism which considered any extrahepatic or biliary elimination (and assumes no extrahepatic metabolic clearance) as reported in eqn (12):

$$f_{met} = 1 - f_{renal} - f_{biliary} \quad (12)$$

The *in vivo* blood clearance was estimated by scaling the metabolic plasma clearance with the blood-to-plasma concentration ratio (R_{BP}):

$$CL_b\ (\text{mL min}^{-1}\ \text{kg}^{-1}) = \frac{CL_{H,p}}{R_{BP}} \quad (13)$$

The observed hepatic intrinsic clearance was estimated by assuming the well-stirred model using eqn (14):[21]

$$CL_{H,int}\ (\text{mL min}^{-1}\ \text{kg}^{-1}) = \frac{CL_b}{\dfrac{fu_{,p}}{R_{BP}}\left(1 - \dfrac{CL_b}{Q_H}\right)} \quad (14)$$

where Q_H is the average hepatic blood flow of 20.7 mL min⁻¹ kg⁻¹.[21]

2.13 Software and libraries for modelling

The *in silico* modelling was performed in R using *RxODE* for simulations and *nlmixr* for model fitting. These libraries are open source and available in the R repository CRAN.

The fitting of diclofenac and quinidine data was performed in Phoenix 64 version 8.2.0.4383 (Certara, New Jersey, US) using naïve pooled as the fitting algorithm.

For models 4, 5, and 6 (Fig. 7) an *a priori* identifiability was performed in the REDUCE language using the open source library DAISY (differential algebra for identifiability of systems).[26,27] The technical application and the codes are reported in the ESI† (Modelling session).

Analytical graphs were generated with GraphPad Prism version 7.04 for Windows (GraphPad Software, La Jolla, CA) and in R using the *ggplot* and *gridExtra* libraries.

3. Results and discussion

3.1 Seeding efficacy and hepatocyte number

In vitro drug metabolism studies mainly explore the biotransformation and transport of drugs by the cells (in contrast to *in vitro* pharmacology and toxicology studies that examine the impact of drug exposure on the cells). In this context, quantification of the hepatocyte seeding efficiency and cell number are important assessments to enable quantitative readouts that are normalized by cell number, such as drug clearance and metabolite formation rates. Accurate knowledge of effective cell number is essential for comparing results between *in vitro* systems, for selection of the most suitable system for a given experiment and for the robustness of the subsequent study design (*e.g.* selection of time points, length of experiment, and analysis of cell lysates). In parallel to seeding the plates (at day – 4), unused cells were counted and the amount of total hepatocyte protein was determined on seven separate occasions. Protein content was consistently between 1.015 and 1.078 mg per million cells in six occasions with one outlier (1.302 mg$_{total}$ $_{protein}$ per million cells; *Z*-score = 2.4). Linear regression showed a strong correlation (R^2 = 0.995) between the amount of total protein and the number of cells, with a mean value of 1.051 ± 0.019 mg$_{total}$ $_{protein}$ per million cells (after excluding one outlier Fig. 2A), consistent with other publications.[28] The number of hepatocytes at day 2 (*i.e.* five days after seeding) in the control wells (*n* = 15) from each experiment (*n* = 5) was on average 260 000 ± 25 000 (CV: 9.3%) and ranged from 230 000 to 310 000 hepatocytes. Comparison of the number of hepatocytes measured in the control wells at day 2 with the number initially seeded at day – 4 showed an average seeding efficiency of 52.0 ± 7.1% (CV: 14%) with values ranging from 39.0 to 66.5% (Fig. 2B). Seeding efficiency was more consistent within experiments than between experiments. Cell number was therefore determined for each experiment using satellite wells reserved for this purpose. Reasons for the incomplete seeding efficiency are unknown, but are thought to be a combination of partial attachment of hepatocytes to the surface of the

scaffold and stress to the hepatocytes during medium exchange. Correction for actual cell number also has important implications for quantitative translation to *in vivo* considering the commonly reported trend of clearance under-prediction.[29]

Production of albumin is frequently used as a marker for hepatocyte-like activity. It was explored here as a non-invasive proxy for cell number determination *via* cell lysis and protein concentration measurement. The mean albumin amount in all experiments (*n* = 5) and wells (*n* = 120) was 10.3 ± 3.7 μg (CV: 36%) at day 2 of the experiment (24 h after media exchange). Normalizing the albumin concentration by the measured number of hepatocytes in the control wells (total *n* = 15), allowed the calculation of the average albumin production rate and was 39 ± 8 μg per day per million cells (CV: 22% with values ranging from 23 to 58 μg per day per million cells). The mean (*n* = 3) albumin production rate in individual experiments measured in satellite wells was 27 ± 3 (CV: 10%), 38 ± 3 (CV: 8%), 45 ± 9 (CV: 20%), 40 ± 3 (CV: 7%), and 37 ± 1 (CV: 2.5%) μg per day per million cells in experiments 1, 2, 3, 4, and 5, respectively (Fig. 2C). This is at the lower boundary of the estimated albumin output of human liver *in vivo* of 37 to 105 μg per day per million cells[30] but superior to albumin production rates reported for hepatocyte spheroids recently.[31] The measurement of hepatocyte number (*via* hepatocyte protein amount determination in the satellite wells of each experiment) and the albumin production in all wells of an experiment allowed the hepatocyte number in each test well to be calculated and used in data processing, to account for any well to well differences in cell number (Fig. 2D). This approach also compensated for potential differences in albumin production over time for the different experiments as albumin amount per million hepatocytes was calculated in each experiment.

3.2 Assessment of drug metabolizing enzyme activities

At very low drug concentrations the rate of drug metabolism is typically proportional to drug concentration, which therefore decreases exponentially with incubation time. Intrinsic clearance (CL$_{int}$) is an absolute measurement parameter calculated from fitting an exponential decay function to the drug concentration *vs.* incubation time data and the parameter of choice for comparison and extrapolation of data between different *in vitro* systems or between *in vitro* and *in vivo*. The intrinsic clearances of four cytochrome P450 (CYP) substrates, seven UDP-glucuronosyl transferase (UGT) substrates, and one aldehyde oxidase (AO) substrate were measured in order to assess the metabolic capabilities of the hepatocyte cultures in the liver-on-a-chip system. Fig. 3 shows the media concentration-time profiles of the drugs. Inter-well variability of the calculated cell number was low and a mean CV of 12% (range from 2 to 21%) was attained. Comparison of measured CL$_{int}$ from the LoC, and leading alternative systems (suspended hepatocytes, and HepatoPac micropatterned cocultured hepatocytes) was

preformed and reported in ESI† Table S6. The CL_{int} values were within 2-fold between liver-on-a-chip and HepatoPac for 8 compounds out of 13. When compared with suspended hepatocytes, CL_{int} values for 11 compounds out of 14 were within 2-fold. For a new system using single donor hepatocytes to compare as well as this to highly optimized pooled hepatocyte test systems indicates the promise of the LoC. Non-specific binding can also cause loss of drug from the media onto device surfaces. It was not assessed in detail in this study since little or no adsorption to the plastic was reported in the available literature for the system[9,32] and as essentially complete recovery of quinidine and diclofenac was recorded in the quantitative experiments. In addition, the presence of BSA in the media also reduces the potential for compound adsorption.[33,34]

3.3 Intrinsic clearance determinations for metabolically stable drugs and application of modelling to control for media sampling and evaporation

In vitro drug metabolism studies monitor drug and metabolite concentrations in quenched incubates or media samples. Multiple samples taken from the media compartment of the liver-on-a-chip system were used to create an *in vitro* PK profile and calculate intrinsic parameters such as drug clearance. Human hepatocyte CL_{int} values are an important selection criterion for drug candidates and are used directly in prediction of human PK. Drugs with low intrinsic clearance (*e.g.* <3 μL per min per million hepatocytes) often exhibit moderate-high *in vivo* stability. In contrast, drugs with high intrinsic clearances may have short *in vivo* half-lives and low bioavailability. Traditional drug metabolism studies using hepatocytes make use of relatively short incubation times and one experimental incubation well per time point which is quenched in its entirety using organic solvent containing internal standard. This treatment largely compensates for evaporation effects because the total drug material is recovered from each well at the end of the experiment. In contrast, organ-on-a-chip systems are likely to have fewer but larger incubation chambers from which multiple samples are removed. Greater consideration of drug amount and concentration within the experiment then becomes important for drug metabolism scientists. The metabolic assessment in the liver-on-a-chip performed here integrates modelling and simulation as a vital part of the study in order to understand in detail what is happening within the experiment and to obtain correct intrinsic clearance estimates. Mathematical modelling was especially needed for the CL_{int} estimations for highly metabolically stable compounds and our study shows the importance of this approach as well as describing under what conditions it is necessary. For the CL_{int} estimation of low turnover compounds an evaporation model was used, which took into account media evaporation (drug concentration and effective cell concentrations increase) and media removal due to sampling (effective cell concentration increases but

drug concentration unchanged). The extent of evaporation was measured for each well separately. The individual well rate of evaporation (k_{ev}) value was used in determination of individual well drug intrinsic clearance before mean values were calculated (eqn (5), for individual well evaporation rates see ESI† Table S4). Experimental data showed significant evaporation (>20%) over 4 days of incubation. Having established the evaporation rate and effect in the liver-on-a-chip system, *in silico* modelling was applied to assess the impact of evaporation on the accuracy of the estimated *in vitro* intrinsic clearance using simulated data (Fig. 4). For the analysis, theoretical concentration-time profiles were simulated using the evaporation model over a range of CL_{int} and k_{ev} values which corresponded to those experimentally observed. Subsequently, both the linear model and the evaporation model were used to assess the simulated concentration-time profiles. Fig. 5 shows the possible bias tackled by the use of the evaporation model and more detailed results are reported in the ESI† (Fig. S4). Not accounting appropriately for evaporation from the media results in significant underestimation of the CL_{int}, in particular for low turnover drugs with CL_{int} below 1 μL per min per million cells and the k_{ev} above 0.05 μL min^{-1} (Fig. S4†). With the simulated experiments, we established in which circumstances of CL_{int} and k_{ev} the linear model needed to be replaced with the more realistic, but also more complex evaporation model (Fig. 5).

In addition, the evaporation model used in the current study also takes into account the media removal due to sampling. Although lorazepam and posaconazole were tested up to 96 h of incubation, the effect of media evaporation was small compared with the rate of drug depletion and the evaporation model did not need to be applied to obtain an accurate CL_{int} estimation. Metabolically stable compounds tested over 96 hours included tolbutamide, irinotecan, and ketoprofen which are CYP2C9,[35] carboxylesterase,[36] and UGT2B7/UGT1A3 (ref. 37) substrates, respectively. From the experimental data reported in Table 2 and the concentration-time profiles shown in Fig. 3D for tolbutamide and irinotecan the inclusion of the measured constant of evaporation in each well and the application of the evaporation model reduced CL_{int} underestimation which would have occurred using a simple linear model up to ~40% (additional information available in Table S4†). (Unfortunately ketoprofen concentration-time data showed high bias dependent upon inclusion of day 1 or day 2 values and was therefore not considered for detailed CL_{int} evaluation and IVIVE). It is important to consider that media evaporation is highly dependent on several factors including the surface area of the well, the humidity of the plate/incubator, air flow around the device and the incubation temperature. The extent of evaporation therefore needs to be determined for each new microphysiological system, its impact on the planned experiments assessed and the relevant data interpretation model implemented.

Table 2 Estimated CL_{int} values of metabolically stable drugs using the evaporation model and the linear model. CL_{int} values are expressed in μL per min per million cells and are reported as mean ± standard deviation from three replicates

Compound	Linear model	Evaporation model
	CL_{int} (μL per min per million cells)	
Tolbutamide	0.41 ± 0.06	0.59 ± 0.07
Irinotecan[a]	0.41 ± 0.03	0.70 ± 0.02

[a] Drug depletion may have occurred also by non-enzymatic activity involving the carbamate moiety at the physiological condition of 37 °C and pH of 7.4. Constant of evaporation (k_{ev}) for each well were reported in Table S4.†

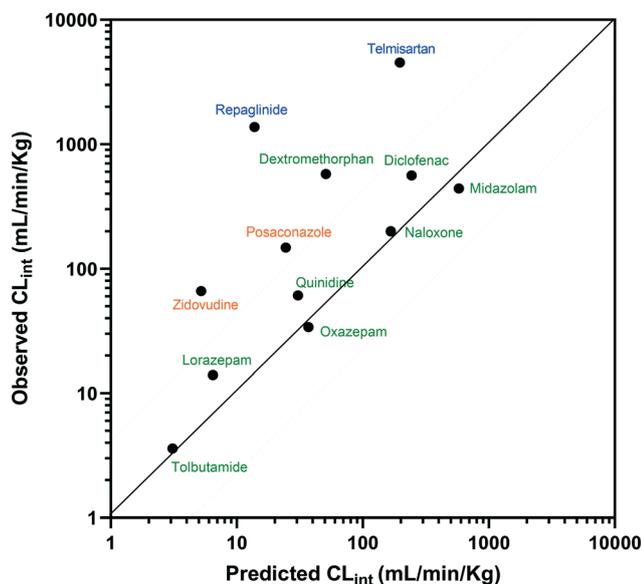### 3.4 Extrapolation of *in vitro* intrinsic clearance to predict *in vivo* intrinsic clearance

The estimated CL_{int} data for 12 of the compounds measured using the liver-on-a-chip were extrapolated to *in vivo* hepatic clearance values using physiologically based scaling. Parameters used for the extrapolation of the *in vitro* clearance data obtained in the liver-on-a-chip for the 12 compounds investigated are reported in Table 1, together with the respective references for the *in vivo* studies. Understanding the translatability of the *in vitro* CL_{int} data to *in vivo* clearance is essential, in order to understand the applicability of the current system and goals for future system enhancements.[29,38] Comparison of extrapolated and observed hepatic *in vivo* CL_{int} values is displayed in Fig. 6. Predicted hepatic intrinsic clearance for 7 out of the 12 substrates used in the analysis (midazolam, quinidine, diclofenac, naloxone,

oxazepam, tolbutamide, and lorazepam) were within 3-fold of the observed data. In particular, the prediction was satisfactory for the more permeable compounds cleared from the body *via* metabolism processes (extended clearance classification system (ECCS) classes 1a and 2). The analysis did not suggest a difference in the prediction success between CYP and UGT substrates.

Zidovudine, dextromethorphan, repaglinide and telmisartan clearance were under-predicted with *in vivo* predicted CL_{int} values <10% of the observed value. Telmisartan[4] and repaglinide[39,40] are substrates of OATP1B3 and OATP1B1, respectively, for which the *in vivo* clearance is likely to be rate-determined by active hepatic uptake prior to biliary elimination. The under-prediction seen for these drugs is in agreement with trends observed for transporter substrates in other 'closed' *in vitro* cellular systems[41] (in which transported drug cannot be eliminated from the test system) and highlights a need for further development of systems capable of mimicking bile flow. Another relevant factor is the use of single donor hepatocytes for the experiments, which may have less than average activities for some metabolic enzymes due to differences in enzyme expression levels or enzyme polymorphisms. The current study demonstrated the application of liver-on-a-chip data for IVIVE of hepatic clearance for a range of CYP and UGT substrates. IVIVE attempts using liver-on-a-chip data have been reported previously, but with a smaller set of drugs.[9] More studies are required to investigate the IVIVE of metabolic clearance based on the PhysioMimix liver-on-a-chip by using a hepatocyte pool containing multiple donors (ideally at least 10 donors) if the system is to represent a population average in a similar manner to recently adopted cellular systems such as micropatterned hepatocyte co-cultures.[20]

Fig. 6 IVIVE of CL_{int} for 12 compounds tested with the liver-on-a-chip and comparison to observed hepatic clearance. Compounds were coloured according to the ECCS classification (class 1a and 2 in green, class 3 in blue, and class 4 in orange). The solid and dotted lines show the line of unity and the interval of ±3-fold, respectively.

3.5 Application of the PhysioMimix liver-on-a-chip to fraction metabolized estimation

The fraction metabolized (f_m) by a given enzyme is an important parameter when trying to estimate inter-individual variability in drug exposure or the magnitude of drug–drug interactions (DDI). For example, if a single metabolic enzyme is responsible for 90% of drug clearance (*i.e.* f_m = 0.9) then drug metabolism can be expected to be reduced 10-fold on inhibition of that enzyme pathway, resulting in elevated exposure and potential toxicity. In contrast, if two or more enzymes contribute equally, full inhibition of one enzyme will maximally reduce the rate of drug metabolism only 2-fold. Several reports have shown that *in vitro* estimated f_m can be combined with physiologically based pharmacokinetic (PBPK) modelling for prediction of clinically reported DDIs.[42,43] The f_m represents a key input parameter in the PBPK modelling and uncertainties in f_m estimates are likely to result in poor predictions of the *in vivo* DDI risk. Determination of fraction metabolized is therefore an important consideration in drug metabolism studies and
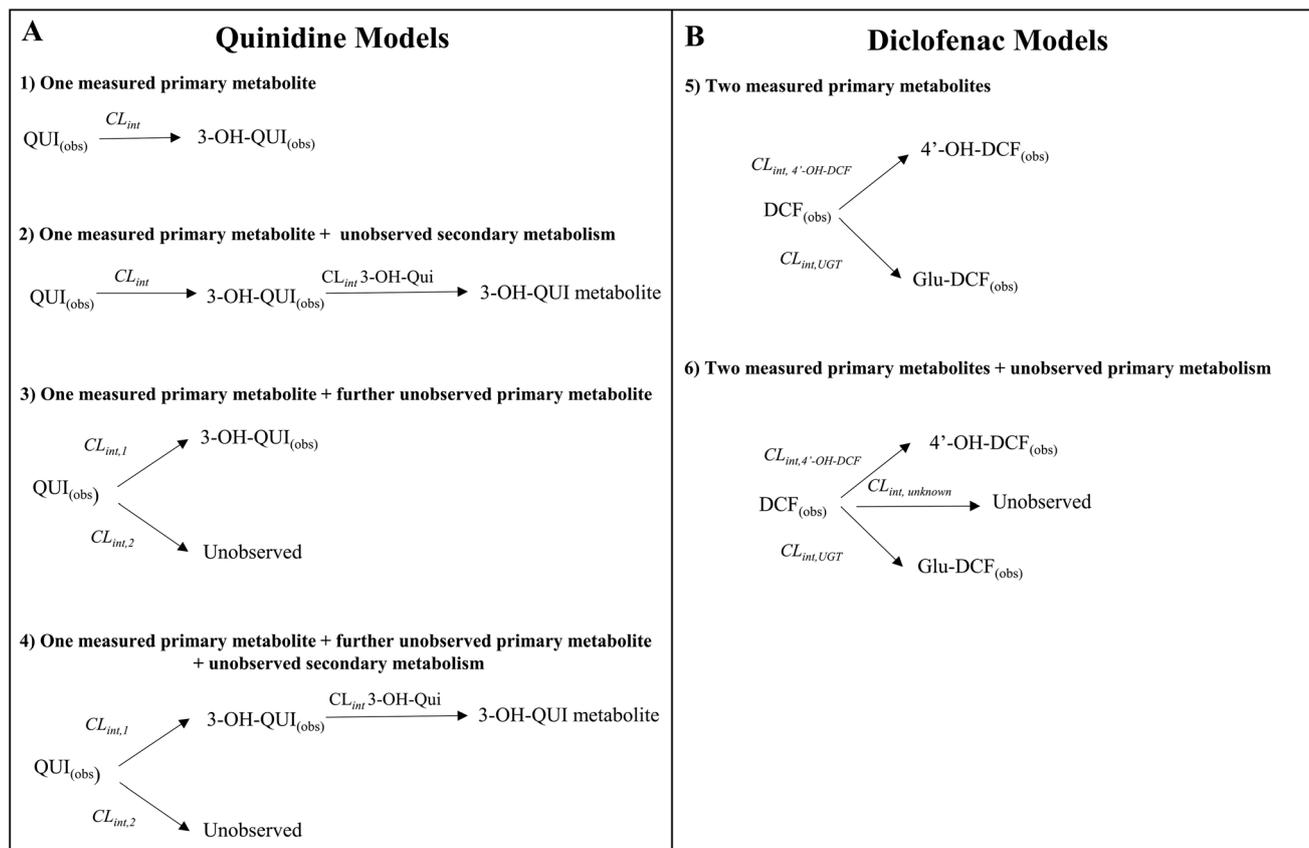
Fig. 7 A) Schematic representation of the metabolic pathways investigated with the *in silico* model for the experimental data of quinidine. B) *In silico* models for the $f_{m,UGT}$ and estimation of diclofenac. The subscript Obs refers to the measured medium concentration of the respective compound.

hepatocyte systems containing a full complement of metabolic enzymes in as physiological environment as possible are the systems of choice for investigating this.

3.5.1 Metabolism pathway analysis for quinidine. Quantitative measurements of the drug (quinidine) and metabolite (3-hydroxyquinidine) concentration-time profiles on day 1 were used to estimate the CL_{int} values of quinidine and the fraction of quinidine metabolized to form 3-hydroxyquinidine (Fig. 8A). Four different models incorporating different metabolic schemes were investigated (Fig. 7A). The simplest model (1), which considered the formation of 3-hydroxyquinidine as the only metabolic pathway did not describe the observed data accurately (Table 3). While models 2 and 3 which considered the further metabolism of 3-hydroxyquinidine and additional metabolism pathways, respectively, both produced good fits to the observed data and showed significantly better BIC values compared to model 1. The more complex model 4 which represents a combination of models 2 and 3 showed similar BIC compared to that of model 3. Whereas model 4 was structurally globally identifiable from *a priori* identifiability study, the estimation of CL_{int} of quinidine and the metabolism of 3-hydroxyquinidine had a quite large uncertainty (~50% for the CL_{int} of 3-hydroxyquinidine) (Table 3). However, the fraction of metabolism proceeding

via the 3-hydroxyquinidine formation pathway estimated from models 3 and 4 provided relatively similar values of 0.64, and 0.71, respectively. The analysis of quinidine data suggested the existence of an additional metabolism pathway besides the measured transformation to the 3-hydroxy metabolite, which might be the N-oxide formation[44] (model 3). Resolution of which model to use therefore requires further data, for instance measurement of quinidine N-oxide formation or of the further metabolism of 3-hydroxyquinidine in the *in vitro* system. However, model 3 might be a likely representation of the actual metabolic profile of quinidine, since available literature reported that the 3-hydroxyquinidine is eliminated without further metabolic transformation in the urine.[16] In order to better distinguish between the various modelling fitting options, a longer incubation without medium change (>24 h) is recommended for a future study. It is anticipated that with extended incubation time and the quantification of quinidine *N*-oxide in addition a better resolution of the optimal model to use may be reached.

3.5.2 Fraction metabolized estimation for diclofenac. A similar investigation was performed with diclofenac which is metabolized to diclofenac-glucuronide mostly by UGT2B7,[45] whereas 4′-hydroxydiclofenac and 5′-hydroxydiclofenac[46] are formed by CYP2C9 and CYP3A4, respectively, with additional

Table 3 Four different models were applied to estimate CL_{int} of quinidine to form 3-hydroxyquinidine, an unobserved clearance pathway, and 3-hydroxyquinidine clearance. The respective BIC associated with all four models are displayed. Each value is reported with the respective ± standard error

| | | CL_{int} | | | |
| | | Qui. → 3-OH-Qui. | Qui. → unobserved | 3-OH-Qui → 3-OH-Qui met | |
Model	BIC	µL per min per million cells	µL per min per million cells	µL per min per million cells	$f_{m(3\text{-OH-Qui Pathway})}$
1	−65.9	8.2 ± 0.5			1.0
2	−75.2	10 ± 2		4.9 ± 1.0	1.0
3	−82.4	7.9 ± 0.4	4.4 ± 0.8		0.64 ± 0.10
4	−81.5	8.6 ± 0.7	3.5 ± 1.0	2.1 ± 1.2	0.71 ± 0.14

contribution from CYP2C8.[46] To our knowledge, we applied for the first time the PhysioMimix liver-on-a-chip in combination with modelling to determine the metabolic contribution of UGTs for diclofenac. The application of the mathematical models enabled simultaneous assessment of different metabolic pathways of diclofenac. Two models (Fig. 7B) were applied to the analysis of diclofenac *in vitro* data to estimate CL_{int} and $f_{m,UGT}$. Model 6 (3 primary metabolic pathways, no subsequent metabolism) was the best model to describe the experimental data (Fig. 8B) based on the BIC (Table 4). The total unbound CL_{int} was 95 ± 9 µL per min per million cells and the $f_{m,UGT}$ value was 0.64. The $f_{m,UGT}$ reported by Kilford *et al.*[17] in the HLM was 0.62, in close agreement with the value estimated in this study. One or more unassessed metabolic pathway(s) in addition to 4'-hydroxydiclofenac and diclofenac glucuronide formation were suggested by modelling to potentially also contribute ~20%

of the drug clearance. Possible explanations include formation of 5'-hydroxydiclofenac but it must also be considered that potential inaccuracies in drug and metabolite quantitation could result in a similar effect. This underlines the need for highly accurate quantification of metabolite formation and drug depletion if f_m estimates are to be made with confidence.

3.6 Application to the efavirenz metabolite identification

Establishing what metabolites are generated from a new drug candidate forms an essential part of drug metabolism studies. As with f_m estimation, hepatocyte systems which contain a full complement of metabolism enzymes are often used. *In vitro* determinations of metabolic clearance and metabolite formation for compounds with a high metabolic stability may require extended incubation of the test drug.
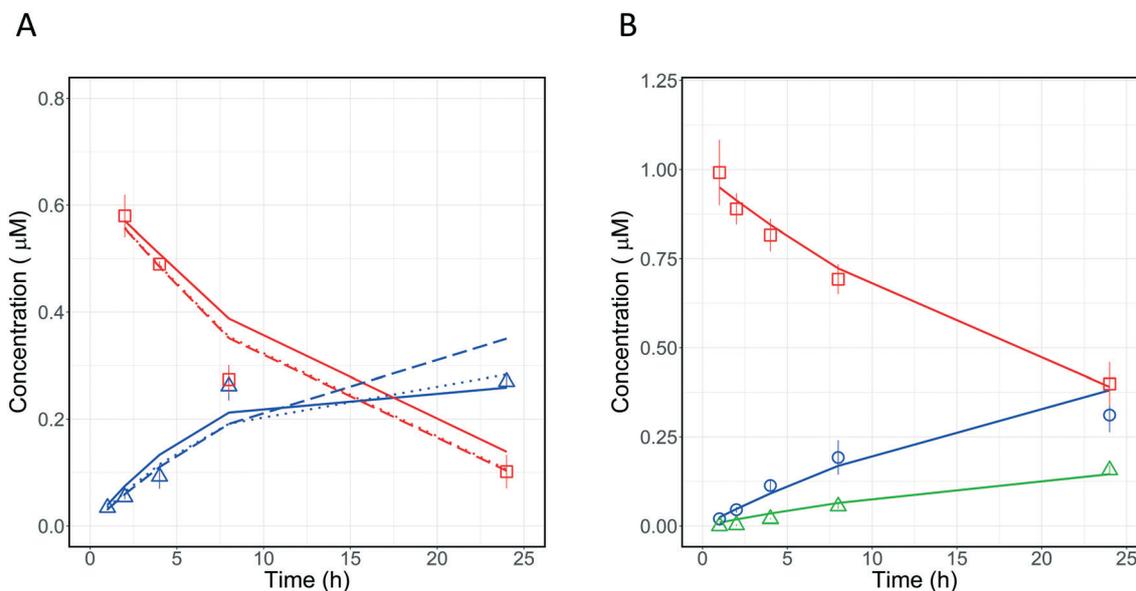
Fig. 8 A) Observed (symbols) and predicted (lines) concentration-time profiles of quinidine and its metabolite 3-hydroxyquinidine on incubation day 1. The experimental data are reported with red squares and blue triangle for quinidine, and 3-hydroxyquinidine, respectively. The fitting profiles from models 2, 3, and 4 are reported with solid, dashed, and dotted line, respectively. B) Comparison of observed (symbols) and predicted (lines) concentration-time profiles of diclofenac and its metabolites 4-hydroxydiclofenac and diclofenac glucuronide on incubation day 1. The experimental data are reported with red squares, blue circles, and green triangles for diclofenac, 4-hydroxydiclofenac, and diclofenac glucuronide, respectively. All experimental data were measured as triplicates and each point represents the mean with the respective standard deviation.

Table 4 Two different models were applied to estimate CL_{int} and $f_{m,UGT}$ of diclofenac. CL_{int} values from the observed metabolites and the unobserved metabolic pathway is displayed together with the estimated $f_{m,UGT}$ for both models. The respective BIC associated with models are displayed to indicate the goodness of the fitting. Each value is reported with the respective ± standard error

| | | CL_{int} | | |
| | | Observed metabolites | Unobserved | |
Model	BIC	µL per min per million cells	µL per min per million cells	$f_{m,UGT}$
5	−178	86 ± 3		0.80 ± 0.03
6	−192	73 ± 4	22 ± 5	0.64 ± 0.02

Standard *in vitro* systems (*e.g.* suspended hepatocytes, liver microsomes) have a rapid decrease in metabolic activity, which may prevent the detection of primary, secondary or tertiary metabolites of low clearance drugs. We selected efavirenz as an example drug with low metabolic turnover and quite complex metabolic pathways with various secondary and tertiary metabolites formed both *in vitro* and *in vivo*[47] (Fig. 9). In addition, efavirenz metabolism represents a good example for metabolite identification investigations because multiple classes of enzymes including CYP isoforms (CYP2B6 with minor contributions from CYPs 1A2, 1A6, 3A4 and 3A5), UGTs (UGT2B7 in the direct *N*-glucuronidation of efavirenz) and sulfotransferases are involved in the primary and further metabolism of the drug.[48] All metabolites reported from in vivo analysis: 8-hydroxyefavirenz (M1), efavirenz-*N*-glucuronide (M5), 8-hydroxyefavirenz-glucuronide (M4) and 7-hydroxyefavirenz glucuronide (M8) were identified

in the liver-on-a-chip system incubates. The metabolite 7-hydroxyefavirenz (M6) was not detected, most likely because of further metabolism, which produced its observed glucuronidated (M8) and sulphated (M7) conjugate metabolites (see ESI† Fig. S5 for time course profiles of efavirenz and all detected metabolites). In addition, secondary metabolism of 8-hydroxyefavirenz to 8-hydroxyefavirenz glucuronide (M4) was detected as well as metabolites formed *via* the hydroxylation of the cyclopropane moiety of 8-hydroxyefavirenz (M2) and further glucuronidation (M3). The pair of regioisomer metabolites M4–M8 were separated by chromatography, although minimal differences in fragmentation and the absence of standards prevented a definitive identification. As almost all metabolites of efavirenz were detected including metabolites from tertiary metabolism, the liver-on-a-chip system might allow for complex metabolite identification studies for the
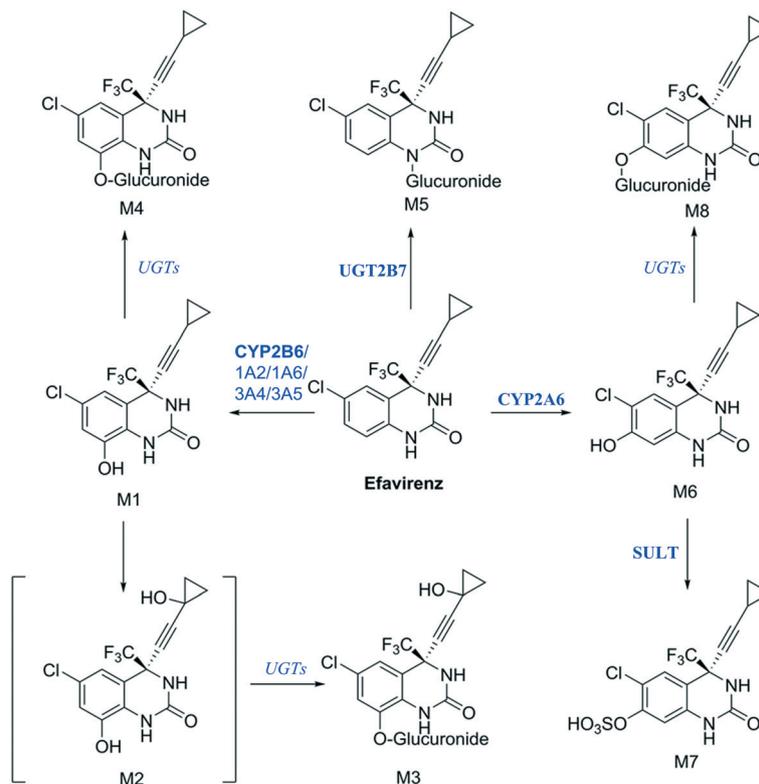
Fig. 9 Proposed efavirenz metabolic pathway from human urine metabolites detection.[47] Above each arrow the metabolic enzymes involved in the reaction are reported. The main enzyme isoforms in the metabolism are reported in bold from Cong Xu *et al.*,[48] and in italic when the specific isoform involved was not available or unknown.

characterization of the preclinical drug candidates. The large media volume allows larger volumes to be taken for multiple analyses and the cell longevity permits to detect metabolites with low formation rates after extended incubation times.

3.7 Opportunities for further liver-on-a-chip system development

A significant loss of 40–50% of the initial metabolic activity has been reported for 2D-monocultured hepatocytes within less than 24 hours after seeding.[1,15] Such a loss of enzyme activity is easily observed in the concentration-time profiles of drugs in the incubations. In each of the intrinsic clearance experiments performed in this study there was no indication of substantive enzyme activity loss during undisturbed incubation, with the potential exception of ketoprofen where the drug depletion profile was less well defined. In order to explore the use of the system further and potentially generate larger amounts of data from the same cells, the retention of drug metabolism capacity on repeated use of the system was assessed for seven drugs using the same cell culture wells but with drug and media replacement each day (see ESI† Fig. S2 and S3 for substrate depletion and metabolite generation profiles, respectively). This experiment may represent a worst case scenario showing the retention of drug metabolizing enzyme activities under harsher cell treatment conditions than were actually applied in the work presented. Nevertheless, it shows the limits of the system usability. It was informative to see that >80% activity was retained on day 2 for all substrates tested, whereas with extended culture time and repeated media exchange the activity was decreased on subsequent days. For substrates mainly metabolized by CYP enzymes (midazolam, dextromethorphan, repaglinide, and quinidine) or AO (carbazeran), the activity at day 4 was between 47–51% of that on day 1, whereas the activity for UGT substrates was better retained with 62% retention for diclofenac and 70% for naloxone (Fig. S2†). These findings were not consistent with the linear *in vitro* PK profiles observed for lorazepam, posaconazole or tolbutamide, incubated over 4 days in undisturbed culture and suggest that daily media removal and replacement may affect the enzyme activities of the hepatocytes. In the case of ketoprofen it is possible that activity loss during extended culture affected the concentration-time profile and therefore intrinsic clearance determination and so it was not used for IVIVE assessments. Decreasing activity in oxidative metabolism was observed in a previous study conducted by Rubiano and colleagues, who reported an approximately 50% decrease in CYP3A4 activity over the first 10 days of culture.[12] Culturing of hepatocytes as spheroids was also subject to activity loss over time,[49] and the choice of medium was highlighted as relevant to retain a stable metabolic activity. Hepatocytes benefit from co-culture with other cells, as exemplified by the HepatoPac or HμREL cultures.[50,51] Both of these systems involve co-culture with fibroblasts, which enable the hepatocytes to survive for multiple weeks with regular media exchange or for up to one week in the absence of media replenishment.[51] Building upon the demonstrated culture benefits of media flow shown in the liver on a chip system, co-culture of hepatocytes in the PhysioMimix system may therefore represent a potential next step in further system development for DMPK applications.

4. Conclusion

Testing of microphysiological systems to establish their cellular performance, suitability for use with today's drug molecules and validation for the proposed application are needed if the systems are to contribute to drug candidate optimization and selection in the pharmaceutical industry. The current investigations demonstrated that measurement of seeding efficiency and quantification of the active cell number using biomarkers such as albumin were essential for quantitative understanding of the system. Having passed basic system suitability assessments, more advanced studies were conducted to explore the merit of the system for DMPK studies. Mathematical modelling of the data enabled more correct results to be obtained by accounting for relevant evaporation from the media over time, particularly for metabolically stable drugs, and enabled simultaneous determinations of clearance and fraction metabolized values. Extrapolation of the *in vitro* clearance to *in vivo* clearance demonstrated that the system already offers reasonable human translatability, although not exceeding that of leading hepatocyte co-culture systems. This work represents a step along the path of liver-on-a-chip optimization and highlights some of the validation aims and approaches relevant to a drug metabolism setting in the pharmaceutical industry. In order to elicit its full potential, future adaptations of the liver-on-a-chip can be envisaged which would further extend the lifetime of drug metabolizing enzyme activities, assess ability to capture transporter-mediated clearance and make use of pooled hepatocyte cultures as representative of population average activities. This should then enable application of liver-on-a-chip to 1) more precise CL_{int} determination for low clearance drugs, 2) prediction of pharmacokinetic variability and drug–drug interactions (in particular in case of metabolism-transporter interplay) and 3) more confidence in detection of active or toxic metabolites prior to clinical development.

Author contributions

Participated in research design: Docci, Milani, Gertz, Galetin, Parrott, Fowler. Conducted experiments: Docci, Milani, Ramp. Performed data analysis: Docci, Milani, Ramp, Romeo, Gertz, Parrott, Fowler. Wrote or contributed to the writing of the manuscript: Docci, Milani, Romeo, Godoy, Ortiz Franyuti, Krähenbühl, Gertz, Galetin, Parrott, Fowler.

Conflicts of interest

Acknowledgements

References

1 C. M. Smith, C. K. Nolan, M. A. Edwards, J. B. Hatfield, T. W. Stewart, S. S. Ferguson, E. L. Lecluyse and J. Sahi, *J. Pharm. Sci.*, 2012, **101**, 3989–4002.

2 S. Fowler, W. L. K. Chen, D. B. Duignan, A. Gupta, N. Hariparsad, J. R. Kenny, W. G. Lai, J. Liras, J. A. Phillips and J. Gan, *Lab Chip*, 2020, **20**, 446–467.

3 E. Kimoto, R. Li, R. J. Scialis, Y. Lai and M. V. Varma, *Mol. Pharmaceutics*, 2015, **12**, 3943–3952.

4 T. De Bruyn, A. Ufuk, C. Cantrill, R. E. Kosa, Y.-A. Bi, M. Niosi, S. Modi, A. D. Rodrigues, L. M. Tremaine and M. V. Varma, *Drug Metab. Dispos.*, 2018, **46**, 989–1000.

5 W. R. Proctor, A. J. Foster, J. Vogt, C. Summers, B. Middleton, M. A. Pilling, D. Shienson, M. Kijanska, S. Strobel, J. M. Kelm, P. Morgan, S. Messner and D. Williams, *Arch. Toxicol.*, 2017, **91**, 2849–2863.

6 M. L. Sutherland, K. M. Fabre and D. A. Tagle, *Stem Cell Res. Ther.*, 2013, **4**(Suppl 1), I1.

7 E. W. Esch, A. Bahinski and D. Huh, *Nat. Rev. Drug Discovery*, 2015, **14**, 248–260.

8 https://cn-bio.com/, (access August 2021).

9 N. Tsamandouras, T. Kostrzewski, C. L. Stokes, L. G. Griffith, D. J. Hughes and M. Cirit, *J. Pharmacol. Exp. Ther.*, 2017, **360**, 95–105.

10 A. Vivares, S. Salle-Lefort, C. Arabeyre-Fabre, R. Ngo, G. Penarier, M. Bremond, P. Moliner, J.-F. Gallas, G. Fabre and S. Klieber, *Xenobiotica*, 2015, **45**, 29–44.

11 U. Sarkar, K. C. Ravindra, E. Large, C. L. Young, D. Rivera-Burgos, J. Yu, M. Cirit, D. J. Hughes, J. S. Wishnok, D. A. Lauffenburger, L. G. Griffith and S. R. Tannenbaum, *Drug Metab. Dispos.*, 2017, **45**, 855–866.

12 A. Rubiano, A. Indapurkar, R. Yokosawa, A. Miedzik, B. Rosenzweig, A. Arefin, C. M. Moulin, K. Dame, N. Hartman and D. A. Volpe, *Clin. Transl. Sci.*, 2020, **14**, 1049–1061.

13 N. Tsamandouras, W. L. K. Chen, C. D. Edington, C. L. Stokes, L. G. Griffith and M. Cirit, *AAPS J.*, 2017, **19**, 1499–1512.

14 M. Tachibana, M. Tanaka, Y. Masubuchi and T. Horie, *Drug Metab. Dispos.*, 2005, **33**, 803.

15 L. Docci, N. Parrott, S. Krahenbuhl and S. Fowler, *SLAS Discovery*, 2019, **24**, 523–536.

16 F. Nielsen, K. K. Nielsen and K. Brøsen, *J. Chromatogr. B: Biomed. Sci. Appl.*, 1994, **660**, 103–110.

17 P. J. Kilford, R. Stringer, B. Sohal, J. B. Houston and A. Galetin, *Drug Metab. Dispos.*, 2009, **37**, 82–89.

18 M. I. Blonk, C. C. Langemeijer, A. P. Colbers, K. E. Hoogtanders, R. H. van Schaik, B. J. Schouwenberg and D. M. Burger, *Antiviral Ther.*, 2016, **21**, 143–152.

19 B. Kaye, J. Offerman, J. Reid, H. Elliott and W. Hillis, *Xenobiotica*, 1984, **14**, 935–945.

20 L. Docci, F. Klammers, A. Ekiciler, B. Molitor, K. Umehara, I. Walter, S. Krähenbühl, N. Parrott and S. Fowler, *AAPS J.*, 2020, **22**, 1–12.

21 M. Gertz, A. Harrison, J. B. Houston and A. Galetin, *Drug Metab. Dispos.*, 2010, **38**, 1147–1158.

22 K. Umehara, C. Cantrill, M. B. Wittwer, E. Di Lenarda, F. Klammers, A. Ekiciler, N. Parrott, S. Fowler and M. Ullah, *Drug Metab. Dispos.*, 2020, **48**, 849–860.

23 L. Docci, F. Klammers, A. Ekiciler, B. Molitor, K. Umehara, I. Walter, S. Krähenbühl, N. Parrott and S. Fowler, *AAPS J.*, 2020, **22**, 131.

24 D. A. Tess, H. Eng, A. S. Kalgutkar, J. Litchfield, D. J. Edmonds, D. A. Griffith and M. V. Varma, *J. Med. Chem.*, 2020, **63**, 11831–11844.

25 H. S. Brown, M. Griffin and J. B. Houston, *Drug Metab. Dispos.*, 2007, **35**, 293–301.

26 M. P. Saccomani and L. D'angiò, *IFAC Proceedings Volumes*, 2009, vol. 42, pp. 48–53.

27 G. Bellu, M. P. Saccomani, S. Audoly and L. D'Angiò, *Comput. Methods Programs Biomed.*, 2007, **88**, 52–61.

28 N. A. Kratochwil, C. Meille, S. Fowler, F. Klammers, A. Ekiciler, B. Molitor, S. Simon, I. Walter, C. McGinnis, J. Walther, B. Leonard, M. Triyatni, H. Javanbakht, C. Funk, F. Schuler, T. Lavé and N. J. Parrott, *AAPS J.*, 2017, **19**, 534–550.

29 F. L. Wood, J. B. Houston and D. Hallifax, *Drug Metab. Dispos.*, 2017, **45**, 1178–1188.

30 A. R. Baudy, M. A. Otieno, P. Hewitt, J. Gan, A. Roth, D. Keller, R. Sura, T. R. Van Vleet and W. R. Proctor, *Lab Chip*, 2020, **20**, 215–225.

31 J. Riede, B. M. Wollmann, E. Molden and M. Ingelman-Sundberg, *Drug Metab. Dispos.*, 2021, **49**, 501–508.

32 P. M. van Midwoud, A. Janse, M. T. Merema, G. M. Groothuis and E. Verpoorte, *Anal. Chem.*, 2012, **84**, 3938–3944.

33 J. I. Wakayama, H. Sekiguchi, S. Akanuma, T. Ohtani and S. Sugiyama, *Anal. Biochem.*, 2008, **380**, 51–58.

34 S. I. Kovalchuk, N. A. Anikanov, O. M. Ivanova, R. H. Ziganshin and V. M. Govorun, *Anal. Chim. Acta*, 2015, **893**, 57–64.

35 C. R. Lee, J. A. Pieper, A. L. Hinderliter, R. F. Frye, J. A. Blaisdell and J. A. Goldstein, *J. Clin. Pharmacol.*, 2003, **43**, 84–91.

36 M. Femke, A. K. Goey, R. H. van Schaik, R. H. Mathijssen and S. Bins, *Clin. Pharmacokinet.*, 2018, **57**, 1229–1254.

37 A. Di Marco, M. D'Antoni, S. Attaccalite, P. Carotenuto and R. Laufer, *Drug Metab. Dispos.*, 2005, **33**, 812–819.

38 A. Galetin, in *Enzyme Kinetics in Drug Metabolism*, Springer, 2014, pp. 255–288.

39 C. Säll, J. B. Houston and A. Galetin, *Drug Metab. Dispos.*, 2012, **40**, 1279–1289.

40 M. Gertz, N. Tsamandouras, C. Säll, J. B. Houston and A. Galetin, *Pharm. Res.*, 2014, **31**, 2367–2382.

41 K. Ménochet, K. E. Kenworthy, J. B. Houston and A. Galetin, *J. Pharmacol. Exp. Ther.*, 2012, **341**, 2.

42 M. Rowland, C. Peck and G. Tucker, *Annu. Rev. Pharmacol. Toxicol.*, 2011, **51**, 45–73.

43 E. Luzon, K. Blake, S. Cole, A. Nordmark, C. Versantvoort and E. G. Berglund, *Clin. Pharmacol. Ther.*, 2017, **102**, 98–105.

44 T. L. Nielsen, B. B. Rasmussen, J.-P. Flinois, P. Beaune and K. Brøsen, *J. Pharmacol. Exp. Ther.*, 1999, **289**, 31–37.

45 K. E. Lazarska, S. J. Dekker, N. P. Vermeulen and J. N. Commandeur, *Toxicol. Lett.*, 2018, **284**, 70–78.

46 T. Wei, *Curr. Drug Metab.*, 2003, **4**, 319–329.

47 A. Mutlib, H. Chen, G. Nemeth, J. Markwalder, S. Seitz, L. Gan and D. Christ, *Drug Metab. Dispos.*, 1999, **27**, 1319–1333.

48 C. Xu, S. K. Quinney, Y. Guo, S. D. Hall, L. Li and Z. Desta, *Drug Metab. Dispos.*, 2013, **41**, 2004–2011.

49 K. P. Kanebratt, A. Janefeldt, L. Vilén, A. Vildhede, K. Samuelsson, L. Milton, A. Björkbom, M. Persson, C. Leandersson and T. B. Andersson, *J. Pharm. Sci.*, 2020, **110**, 422–431.

50 P. Chao, T. Maguire, E. Novik, K.-C. Cheng and M. Yarmush, *Biochem. Pharmacol.*, 2009, **78**, 625–632.

51 U. Zanelli, N. P. Caradonna, D. Hallifax, E. Turlizzi and J. B. Houston, *Drug Metab. Dispos.*, 2012, **40**, 104–110.

52 M. Zientek, Y. Jiang, K. Youdim and R. S. Obach, *Drug Metab. Dispos.*, 2010, **38**, 1322–1327.

53 A. Yu and R. L. Haining, *Drug Metab. Dispos.*, 2001, **29**, 1514–1520.

54 W. Tang, *Curr. Drug Metab.*, 2003, **4**, 319–329.

55 V. Uchaipichat, C. Suthisisang and J. O. Miners, *Drug Metab. Dispos.*, 2013, **41**, 1273.

56 Y. S. Lin, A. L. Dowling, S. D. Quigley, F. M. Farin, J. Zhang, J. Lamba, E. G. Schuetz and K. E. Thummel, *Mol. Pharmacol.*, 2002, **62**, 162–172.

57 M. H. Court, S. X. Duan, C. Guillemette, K. Journault, S. Krishnaswamy, L. L. Von Moltke and D. J. Greenblatt, *Drug Metab. Dispos.*, 2002, **30**, 1257–1265.

58 A. Ghosal, N. Hapangama, Y. Yuan, J. Achanfuo-Yeboah, R. Iannucci, S. Chowdhury, K. Alton, J. E. Patrick and S. Zbaida, *Drug Metab. Dispos.*, 2004, **32**, 267.

59 T. L. Nielsen, B. B. Rasmussen, J.-P. Flinois, P. Beaune and K. Brøsen, *J. Pharmacol. Exp. Ther.*, 1999, **289**, 31.

60 T. B. Bidstrup, I. Bjørnsdottir, U. G. Sidelmann, M. S. Thomsen and K. T. Hansen, *Br. J. Clin. Pharmacol.*, 2003, **56**, 305–314.

61 A. Yamada, K. Maeda, N. Ishiguro, Y. Tsuda, T. Igarashi, T. Ebner, W. Roth, S. Ikushiro and Y. Sugiyama, *Pharmacogenet. Genomics*, 2011, **21**, 523–530.

62 O. Barbier, D. Turgeon, C. Girard, M. D. Green, T. R. Tephly, D. W. Hum and A. Bélanger, *Drug Metab. Dispos.*, 2000, **28**, 497–502.

63 J. D. Lutz and N. Isoherranen, *Drug Metab. Dispos.*, 2012, **40**, 159–168.

64 A. R. Silva and R. J. Dinis-Oliveira, *Drug Metab. Rev.*, 2020, **52**, 258–282.